Future changes in Beijing haze events under different anthropogenic aerosol emission scenarios

Lixia Zhang[1,2], Laura J. Wilcox[3], Nick J. Dunstone[4], David J. Paynter[5], Shuai Hu[1,6], Massimo Bollasina[7], Donghuan Li[9], Jonathan K. P. Shonk[3,8], and Liwei Zou[1]

1 LASG, Institute of Atmospheric Physics, Chinese Academy of Sciences, Beijing, China

2 Collaborative Innovation Center on Forecast and Evaluation of Meteorological Disasters, Nanjing University of Information Science & Technology, Nanjing, 210044, China

3 National Centre for Atmospheric Science, Department of Meteorology, University of Reading, UK

4 Met Office Hadley Centre, FitzRoy Road, Exeter EX1 3PB, UK

5 NOAA/Geophysical Fluid Dynamics Laboratory, Princeton, New Jersey

6 University of Chinese Academy of Sciences, Beijing 100049, China

7 School of Geosciences, Grant Institute, University of Edinburgh, Edinburgh, UK

8 Now at: MetOffice@Reading, Department of Meteorology, University of Reading, UK

9 Key Laboratory of Water Cycle and Related Land Surface Processes, Institute of Geographic Sciences and Natural Resources Research, Chinese Academy of Sciences

Submitted to Atmospheric Chemistry and Physics

Revised on 17th Jan, 2021

Deleted: 10

Deleted: *Sep*

Deleted: *0*

Corresponding author: Dr. Lixia Zhang

LASG, Institute of Atmospheric Physics, Chinese Academy of Sciences, Beijing 100029, China

Phone: 86-10-8299-5456 Email: lixiazhang@mail.iap.ac.cn

Abstract: Air pollution is a major issue in China and one of the largest threats to public health. We investigated future changes in atmospheric circulation patterns associated with haze events in the Beijing region, and the severity of haze events during these circulation conditions, from 2016 to 2049 under two different aerosol scenarios: a maximum technically feasible aerosol reduction (MTFR) and a current legislation aerosol scenario (CLE). In both cases greenhouse gas emissions follow the Representative Concentration Pathway (RCP) 4.5. Under RCP4.5 with CLE aerosol the frequency of circulation patterns associated with haze events increases due to a weakening of the East Asian winter monsoon via increased sea level pressure over the North Pacific. The rapid reduction in anthropogenic aerosol and precursor emissions in MTFR further increases the frequency of circulation patterns associated with haze events, due to further increases of the sea level pressure over the North Pacific and a reduction in the intensity of the Siberian high. Even with the aggressive aerosol reductions in MTFR periods of poor visibility, represented by above normal aerosol optical depth (AOD), still occur in conjunction with haze-favorable atmospheric circulation. However, the intensity of poor visibility decreases in MTFR, so that haze events are less dangerous in this scenario by 2050 compared to CLE, and relative to the current baseline. This study reveals the competing effects of aerosol emission reductions on future haze events through their direct contribution to haze and their influence on the atmospheric circulation patterns. A compound consideration of these two impacts should be taken in future policy making.

Deleted: atmospheric circulation patterns currently associated with haze in the current climate

Key Words: air-pollution, anthropogenic aerosol, atmospheric circulation, haze events

1. Introduction

The increases in aerosol and precursor emissions in China due to the rapid economic development and urbanization in recent decades have caused more frequent and severe haze events. Beijing and the surrounding area is the most polluted region in China (Niu et al., 2010; Ding and Liu, 2014; An et al., 2019; Chen and Wang, 2015). Air pollution has become one of the major issues in China, and the greatest threat to public health. Since the implementation of the "Atmospheric Pollution Prevention and Control Action Plan" in 2013 (China State Council, 2013), aerosol emissions have dramatically decreased, with sulfur dioxide (SO_2) reduced by 59% in 2017 compared to 2013 (Zheng et al., 2018). However, haze events have still occurred regularly in recent years, as, in addition to being influenced by aerosol emissions, meteorological conditions, including limited scavenging, dispersion and ventilation, have been found to play important roles in the variation of air-quality in northern China (An et al., 2019; Pei et al., 2018; Cai et al., 2017). Such events are typically associated with the occurrence of large-scale atmospheric circulation patterns favoring the accumulation of pollutants (Chen and Wang, 2015; Zhang et al., 2014). Locally, a strong temperature inversion in the lower troposphere, weak surface winds, and subsiding air in the planetary boundary layer are favorable for the development and persistence of haze events (Wu et al., 2017; Feng et al., 2018). As anthropogenic aerosol has the potential to induce changes in the atmospheric circulation, in addition to making a direct contribution to the chemical composition of haze, it is crucial to understand how changes in aerosol emissions might

Formatted: Indent: First line: 0 ch

Deleted: (Wang et al., 2013; Chen and Wang, 2015)

Deleted: 5

Formatted: Font color: R,G,B (4,50,255)

Deleted: ph

Deleted: 5

Deleted: Chen and Wang, 2015;

Deleted: Yan et al., 2018

contribute to the frequency and intensity of haze events in future.

On interannual time scales, the East Asian winter monsoon (EAWM) is significantly negatively correlated with aerosol concentrations in Beijing, due to the associated high frequency of extreme anomalous southerly episodes in North China, a weakened East Asian trough in the mid-troposphere and a northward shift of the East Asian jet stream in the upper troposphere (Jeong and Part, 2017; Li et al., 2016; Pei et al., 2018). The cold air process over Beijing is favorable for pollutant dispersion and transport outside because of the accompanied large near-surface wind speed and deep mixing layer. A low occurrence of cold air processes in the recent winters of 2013, 2014 and 2017 has resulted in severe pollution (He et al., 2018). In past decades, the weakening of the EAWM was found to contribute to the increased frequency of haze events over North China (Chen and Wang, 2015; An et al., 2015). Arctic sea ice extent also has been linked to increased stability over eastern China and has been shown to explain 45%~67% of the interannual to interdecadal variability of winter haze days over eastern China (Wang et al., 2015). Overall, around half of the variability in the frequency of haze events in Beijing is controlled by meteorological conditions, while both meteorological conditions and aerosol emissions contribute to the intensity (Pei et al., 2020). Internal climate variability has contributed to the rapid increase of early winter haze days in North China since 2010 (Zhang et al., 2020).

Formatted: Font color: R,G,B (4,50,255)

Formatted: Font color: R,G,B (4,50,255)

Anthropogenic forcing, estimated by using large ensemble runs with and without anthropogenic forcings, has increased the probability of the atmospheric patterns conducive to severe haze in Beijing by weakening the EAWM (Li et al., 2018). Projections based on Coupled Model Intercomparison Project Phase 5 (CMIP5) models showed that weather conditions conducive to haze events in Beijing will increase with global warming due to an increased occurrence of stagnation days in response to both accelerated Arctic ice melting (Cai et al., 2017; Liu et al., 2019a) and a continued weakening of EAWM (Hori et al., 2006; Pei et al., 2018; Liu et al., 2019a). If there is no change in aerosol emission in future, increased stagnation days and decreased light precipitation days associated with global warming would also cause an increase in air pollution days in eastern China (Chen et al., 2019). Regional climate model simulations under the RCP4.5 scenario showed that the air environment carrying capacity, a combined metric measuring the capacity of the atmosphere to transport and dilute pollutants, tends to decrease in the 21st century across China (Han et al., 2017). However, there is large uncertainty in future aerosol emission pathways, with uncertainty around the sign of the change in global emission rate, as well as choice of haze index, and internal climate variability (Scannell et al., 2019; Callahan et al., 2019; Callahan and Mankin, 2020). Furthermore, changes in aerosol emission may influence haze events through their influence on the large-scale atmospheric circulation, in addition to their role in haze composition.

Deleted: as well as the magnitude of the change

The interplay between the role of aerosol as a constituent of haze, and as a potential driver of changes in the circulation patterns conducive to haze, have yet to be explored. If the rapid reductions in aerosol and precursor emissions currently underway in China continue in future, understanding the balance between the different influences of anthropogenic aerosol on haze events is a key question. Typically, anthropogenic aerosol (AA) and greenhouse gases (GHGs) both vary in future simulations (e.g. those following the RCPs or Shared Socioeconomic Pathways), which can make their relative contributions difficult to determine. In this work, we examine future scenarios with the same GHGs emission pathway but different aerosol pathways in order to separate these two contributions to changes in Beijing haze events. We address the following two questions: 1) Do the atmospheric conditions conducive to haze events change differently under different AA scenarios? 2) If so, how AA forcing modulate the frequency of haze-favorable circulation and the severity of the haze events change?

The remainder of the paper is organized as follows: we briefly introduce the experiment design and methods in Section 2, and show the atmospheric circulation patterns conducive to Beijing haze events in Section 3. Projected Beijing haze events under two different aerosol emissions and the underlying mechanism of projected circulation changes will be given in Section 4. We will finally provide the summary and discussion in Section 5.

2. Experiments and methods

2.1 Data and experiment design

We use observed daily visibility, relative humidity and wind speed from 1974 to 2013 from the National Climatic Data Center (NCDC) Global Surface Summary of the Day

Deleted: three

Deleted: 1) Do the atmospheric conditions conducive to haze events change in future? 2) Do aerosol reductions contribute to this change? 3) If the frequency of atmospheric conditions conducive to haze events increases in future, do local aerosol reductions act to moderate the severity of the haze events

Deleted: model performance in simulating

Formatted: Font color: R,G,B (4,50,255)

Deleted: E

Formatted: Indent: First line: 0 cm

(GSOD) database (Fig.S1a). Haze days are defined as days with daily visibility less than 10km, relative humidity less than 90% and surface wind speed less than 7m s-1 (Chen and Wang, 2015). The observed haze occurrence is the number of haze days, and observed haze intensity is defined as the minimum 3-day consecutive visibility (VN3day). Spatial distributions of winter mean haze occurrence and VN3day are shown in Fig.S1b-c. Data from the Japanese 55-year Reanalysis (JRA55; Kobayashi et al., 2015) dataset for the period 1958-2013 are used in this study to evaluate the model representations of the present-day climate. The variations of haze index derived from JRA-55 are highly consistent with those from NCEP-NCAR reanalysis (not shown). We only use JRA-55 in this study.

Simulations with the Met Office Unified Model (Global Coupled configuration 2) HadGEM3-GC2 (Williams et al., 2015) and the NOAA Geophysical Fluid Dynamics Laboratory (GFDL) Climate Model version 3 (GFDL-CM3, Donner et al. 2011; Griffies et al. 2011) are used to investigate the impact of different aerosol forcing scenarios. HadGEM3-GC2 is run with a horizontal resolution of N216 (~60 km) in the atmosphere, and ¼° in the ocean. GFDL-CM3 has a horizontal resolution of ~200 km in the atmosphere and 1° in the ocean. Both models include a representation of aerosol-cloud interactions (Ming et al., 2006; Bellouin et al., 2011).

Three sets of experiments were carried out with each model (Table S1): a historical experiment from 1965 to 2014 and two experiments for the future (2016-2050). In the historical experiment, greenhouse gases and anthropogenic aerosol and precursor

Moved (insertion) [1]

Deleted: .

Deleted: We use

Deleted: s

Formatted: Font color: R,G,B (4,50,255)

Moved down [2]: GFDL-CM3 has a horizontal resolution of ~200 km in the atmosphere and 1° in the ocean.

Moved (insertion) [2]

Deleted: 07

Deleted: We employed two models to check the robustness of the results.

Deleted: (His)

Deleted: 2015

Formatted: Font color: R,G,B (4,50,255)

Deleted: 49

emissions are taken from CMIP5 (Lamarque et al., 2010, Taylor et al., 2012). The future experiments have common GHG emissions following the RCP4.5 scenario, but different aerosol emission pathways. The aerosol pathways are the current legislation emissions (CLE) and the maximum technically feasible reduction (MTFR) taken from the ECLIPSE V5a global emission dataset (Amann et al., 2015, https://iiasa.ac.at/web/home/research/researchPrograms/air/ECLIPSEv5a.html). In CLE, anthropogenic aerosol emissions are assumed to evolve following the current legislation, resulting in a moderate global increase by 2050. In contrast, MTFR assumes a full implementation of the most advanced technology presently available to reduce aerosol emissions by 2030, which results in their rapid global decrease over this period. The regional changes in AA for His, CLE and MTFR can be found in Scannell et al. (2019) and Luo et al. (2020).

We use 1980-2004 as a baseline (His), 2016-2049 as the future period, and display anomalies between the two. Compared with His, CLE shows a dramatic increase in SO_2 over Asia, with peak values over India (not shown) and eastern China (Fig. S2a). MTFR has similar changes over Europe to CLE, negligible changes over India (not shown), and a dipole over China, with a weak increase to the north and a decrease to the south (Fig. S2b). Thus, a dramatic decrease in SO_2 in MTFR relative to CLE is seen over the whole Asian continent, particularly over the Beijing region (Fig. S2c).

2.2 Haze weather index and East Asian winter monsoon index

Formatted: Font color: R,G,B (4,50,255)

Deleted: The difference between the future and baseline winter (December to February) mean SO_2 emissions over China is shown in Fig.S1 for CLE and MTFR.

Formatted: Font color: R,G,B (4,50,255)

Deleted: S1a

Formatted: Font color: R,G,B (4,50,255)

Deleted: (not shown)

Formatted: Font color: R,G,B (4,50,255)

Deleted: S1b

Formatted: Font color: R,G,B (4,50,255)

Deleted: 30-45°N, 100-120°E;

Deleted: S1c

Formatted: Font color: R,G,B (4,50,255)

Deleted:

Moved up [1]: Data from the Japanese 55-year Reanalysis (JRA55; Kobayashi et al., 2015) dataset for the period 1958-2013 are used in this study to evaluate the model representations of the present-day climate.

Deleted: W

Deleted: I

Formatted: Font color: R,G,B (4,50,255)

We focus on haze events during the winter (December-February) around Beijing where Chinese haze events are most frequent and severe (Niu et al., 2010; Chen and Wang, 2015). In this study, we use the haze weather index (HWI) proposed by Cai et al. (2017) as it has also been shown to have a strong relationship with PM2.5 concentrations in Beijing.

The HWI comprises three constituent terms representing the vertical temperature gradient in the troposphere (ΔT), the 850-hPa meridional wind (V850), and the north—south shear in the 500-hPa zonal wind (U500) (see boxes and lines in Fig.1). ΔT is calculated as the difference between the 850 hPa temperature averaged over (32.5°–45°N, 112.5°–132.5°E) and the 250-hPa temperature averaged over (37.5°–45°N, 122.5°–137.5°E). V850 is the 850hPa meridional wind averaged over the broader Beijing region (30°–47.5°N, 115°–130°E), and U500 is a latitudinal difference between the 500-hPa zonal wind averaged over a region to the north of Beijing (42.5°–52.5° N, 110°–137.5°E) and a region to the south (27.5°–37.5°N, 110°–137.5°E). Each of the three terms is normalized by their standard deviation over the reference period (here 1980-2004). The three variables are added together to create the HWI, which is then normalized again by its standard deviation over the reference period. A positive HWI represents conditions that are unfavorable to air-pollutant dispersion, and days with HWI>0 are regarded as "haze events". The HWI defined by Cai et al. (2017) made use of daily data. Due to unavailability of model data at daily resolution, we instead used

Formatted: Indent: First line: 0 cm

Deleted: Several large-scale metrics have been proposed to identify haze events (Ding et al., 2017; Feng et al., 2019; Pei et al., 2018).

Deleted: In general, Beijing haze events are accompanied by weaker surface winds, high atmospheric stability, and fewer cold air outbreaks. To capture all of these features in a single metric monthly data. The reliability of using HWI calculated from monthly mean variables will be discussed in Section 3 based on reanalysis.

The strength of the EAWM index is quantified using the index defined by Wang and Chen (2014). This index takes into account both the east-west and the north-south pressure gradients and is defined as:

$$EAWM=(2*SLP_1-SLP_2-SLP_3)/2$$

where SLP_1, SLP_2 and SLP_3 represent normalized sea level pressure (SLP) averaged over Siberia (40-60°N, 70-120°E), the North Pacific (30-50°N, 140°E-170°W) and the Maritime Continent (20°S-10°N, 110-160°E), respectively (see the boxes in Fig. S3). The three components are converted to anomalies and normalized by their standard deviation over the reference period (here 1980-2004). As the EAWM is directly linked to the occurrence of favorable conditions for haze in Beijing (Pei et al. 2018; Liu et al. 2019; Hori et al. 2006), we therefore use this index as an additional metric (using different variables to the HWI) to assess the potential for changes in future haze events under the CLE and MTFR scenarios, and confirm the robustness of the changes indicated by HWI.

2.3 Significance test

To test whether projected winter mean HWI change and frequency of month with HWI≥1 are statistically significant, we estimated internal variability by performing bootstrapped samples. This resampling-based procedure involves three steps. First, we

Formatted: Font color: R,G,B (4,50,255)

Deleted: **2.3 East Asian winter monsoon index**

Formatted: Indent: First line: 0 cm

Deleted: S2

Formatted: Font color: R,G,B (4,50,255)

Formatted: Font:Bold, Font color: R,G,B (4,50,255) randomly select 75-month (135-month), i.e. 25-yr (45-yr) winters, from His (projections), and calculate the mean HWI change of the 75-month relative to His or frequency of month with HWI≥1 of the 75-month. The 75-month and 135-month are selected to mimic any 25-yr in the period 1980-2004 and 45-yr in 2016–2050, respectively; We repeat the first step 2000 times, and the 2000 bootstrapped samples can be viewed as internal variability of His or future projections. We then compare the results of model ensemble mean with the 2000 bootstrapped samples. If it falls outside the top 5% of the distribution, we then claim that the projected changes in mean HWI or frequency of month with HWI≥1 are statistically significant at the 5% level and beyond the variability of internal variability. We also employed a two-sample Kolmogorov-Smirnov test to determine if the probability density function (PDF) distributions are significantly different (Chakravarti et al., 1967).

3. Climatic conditions associated with Beijing haze events

The circulation anomalies averaged over the days with daily HWI>0 are shown in Fig.1a, c, e. The vertical temperature profile shows warmer air at the lower to mid-levels, centered around 850hPa and cold anomalies aloft 250hPa (Fig.1a). Thus, the atmosphere is stable, unfavorable for the vertical dispersion of pollutants. At the mid-latitude (500hPa), we see northward shifted mid-level westerly jets (Fig.1c). The weakened westerly winds along 30°N inhibit the horizontal dispersion of pollutants in Beijing. At the lower-level, the anomalous southerly winds at 850hPa along the East Asian coast lead to a reduction in the prevailing surface cold northerlies in winter

Formatted: Indent: First line: 0 ch

Deleted: greater than 1.0

Deleted:

(Fig.1e). This reduction favors warmer conditions at lower levels and increased moisture over Beijing, thus increasing the likelihood of haze formation and maintenance.

The HWI was defined based on daily data. Due to limitations in data availability, we instead used monthly data to calculate HWI. To determine the reliability of this approach, we first examined the relationship between the magnitude of HWI calculated from monthly data (HWI-month) and the number of days with daily HWI (HWI-daily) > 0 in the JRA-55 reanalysis during the period 1958-2013 (Fig. 2a-b). Changes in HWI-month are highly consistent with those in number of days with HWI-daily>0 (r = 0.97). When HWI-month is greater than 0, about 50% days in that month are recognized with HWI-daily>0, and up to 62% days with HWI-daily >0 when HWI-month ≥ 1.0. In this study, we define favorable climatic conditions of haze events as a month where HWI-month ≥ 1.

We also checked the observed winter haze occurrence and intensity (VN3day) anomalies when HWI-month ≥1. More haze occurrence and reduced visibility are observed over North China, indicating the reliability of using HWI-month≥ 1 as a proxy of the favorable climatic conditions for the haze events in Beijing and the surrounding region. The selection of a higher threshold of HWI-month (e.g. 1.5) does not make a great difference to our results (not shown). The circulation anomalies averaged over HWI-month ≥ 1 (Fig. 1b, d, f) and HWI-daily > 0 (Fig. 1a, c, e) are also consistent with each other, except that the anomalies for HWI-month≥1 are weaker, as would be

Formatted: Font color: R,G,B (4,50,255)

Formatted: Font color: R,G,B (4,50,255)

Deleted: haze events

Deleted: The scatter plots between HWI-monthly and the monthly mean of HWI-daily also demonstrates their high correlation (0.98).

Deleted: as haze days

Formatted: Font color: R,G,B (4,50,255)

Deleted: a

Deleted: ‘

Deleted: ’

Formatted: Font color: R,G,B (4,50,255)

Deleted: , as around 62% of days within this month are likely to be haze days expected. The spatial and temporal consistency of HWI anomalies calculated from monthly and daily data confirms the suitability of our use of monthly data to explore changes in the frequency of Beijing haze events associated circulation. In the following sections, we will use HWI in short for HWI-month.

4. Changes in Beijing haze events under two AA emission scenarios

4.1 Changes in the frequency of circulation patterns conducive to haze events

Both HadGEM3-GC2 and GFDL-CM3 well simulate the key spatial features of the large-scale atmospheric circulation in winter, when compared to JRA-55 for 1980-2004 (Fig.S4). Key features include the westerly jet along 30°N, the East Asian trough, and northerly winds along the East Asian coast, which are caused by the zonal thermal contrast and subsequent pressure gradient between the North Pacific and the Eurasian continent. The models can also reliably capture the vertical temperature difference, the weaker East Asian trough and the anomalous 850-hPa southerly winds associated with haze events (Fig.S5 and Fig.1). The good performance of HadGEM3-GC2 and GFDL-CM3 in simulating the winter monsoon and haze-favorable circulation justifies the use of these two models to estimate HWI changes.

There is a large interannual variability in HWI, and thus no significant trend in HWI either in His, CLE or MTFR (Figures not shown). However, the two models both show an increase in the mean HWI with no consistent change in the standard deviation (Fig.3a, c). The mean HWI in His (1980-2004), CLE (2016-2050) and MTFR (2016-2050) is

Deleted: Both HadGEM3-GC2 and GFDL-CM3 well simulate the key spatial features of the large-scale atmospheric circulation in winter, when compared to JRA-55 for 1980-2004 (Fig.S3). Key features include the westerly jet along 30°N, the East Asian trough, and northerly winds along the East Asian coast, which are caused by the zonal thermal contrast and subsequent pressure gradient between the North Pacific and the Eurasian continent. The models can also reliably capture the vertical temperature difference, the weaker East Asian trough and the anomalous 500-hPa southerly winds associated with haze events (Fig.S4). The good performance of HadGEM3-GC2 and GFDL-CM3 in simulating the climate mean state demonstrates their suitability to explore the changes in circulation patterns associated with haze events under different AA emission scenarios.

Formatted: Font color: R,G,B (4,50,255)

Formatted: Font color: R,G,B (4,50,255)

Formatted: Font color: R,G,B (4,50,255)

Deleted: The time series of winter HWI in the historical simulation and two different future scenarios from each member of HadGEM3-GC2 and GFDL-CM3 are shown in Fig.3a-b.

Formatted: List Paragraph, Indent: First line: 0 cm

Deleted: the index

Formatted: Font color: R,G,B (4,50,255)

Formatted: Font color: R,G,B (4,50,255)

Formatted: Font color: R,G,B (4,50,255)

Deleted: 2014

Formatted: Font color: R,G,B (4,50,255)

Deleted: 49

Deleted: 49

0.00, 0.39, and 0.65 in HadGEM3-GC2. In GFDL-CM3 it is 0, 0.46, and 0.60. A slight increase in the standard deviation of HWI is simulated by HadGEM3-GC2 from His (1.0) and CLE (1.0) to MTFR (1.06), while no change is seen in GFDL-CM3. The occurrence of positive HWI in CLE and MTFR increases relative to His in both models. In both models, the PDF distributions of HWI in His and CLE are significantly different at the 1% level using a Kolmogorov-Smirnov test. The distributions of HWI in CLE and MTFR are also significantly different at the 1% level in HadGEM3-GC2, but insignificant in GFDL-CM3. The changes in the frequency of different HWI bins can be found from the cumulative distribution function (CDF) of HWI (Fig.3b, d). The frequency of HWI≥1 for His, CLE and MTFR is ~18% (16%), 28% (31%), and 34% (37%) in HadGEM3-GC2 (GFDL-CM3), respectively. If AA emissions follow the CLE scenario, the frequency with HWI ≥ 1 will increase by 10% and 15% in HadGEM3-GC2 and GFDL-CM3 respectively. The rapid reduction in AA emissions in MTFR contributes to an extra 6% increase in HWI relative to CLE in both models.

We used a bootstrapping approach to test whether the mean winter HWI changes and to determine whether the frequency of month with HWI≥1 among His, CLE and MTFR are significantly different from each other (Fig.4). The difference in mean HWI between CLE vs His, MTFR vs His, and CLE vs MTFR, are also statistically significant at the 5% level in both models (Fig.4a-b). The frequency of month with HWI≥1 in CLE and MTFR are both statistically different from that in His in the two models, while only in HadGEM3-GC2 simulations is the frequency in MTFR statistically significant from

Deleted: 40
Formatted: Font color: R,G,B (4,50,255)
Deleted: 0… and 0.6053… A slight increase in the standard deviation of HWI is simulated by HadGEM3-GC2 from His (1.0) and CLE (1.0) to MTFR (1.06), while no change is seen ... [1]
Formatted: Font color: R,G,B (4,50,255)
Formatted: Font:(Default) Times New Roman
Deleted: , as shown in Fig.3c-d… We find a shift of the ... [2]
Deleted: distributions
Formatted ... [3]
Formatted ... [4]
Deleted: , although GFDL-CM3 shows a much larger ... [5]
Formatted ... [6]
Deleted: 6
Formatted: Font:(Default) Times New Roman
Deleted: 5.7
Deleted: .6… (3127.3 ... [7]
Formatted: Font:(Default) Times New Roman
Deleted: 5….7 ... [8]
Formatted: Font:(Default) Times New Roman
Formatted: Font:(Default) Times New Roman
Deleted: 4.6
Formatted: Font:(Default) Times New Roman
Deleted: of
Formatted ... [9]
Deleted: 2.6
Formatted: Font:(Default) Times New Roman
Deleted: 11.6
Formatted ... [10]
Deleted: 7
Formatted ... [11]
Deleted:
Deleted: both models
Formatted: Font color: R,G,B (4,50,255)
Formatted: Font:(Default) Times New Roman
Formatted: Indent: First line: 0 ch

that in CLE at the 5% level (Fig. 4c-d).

An examination of the future changes in each component of the HWI is shown in Fig. S6. The shift of HWI towards more positive values from His to CLE, with a larger shift in MTFR relative to His, is found in all three components except that in V850 of GFDL-CM3. The distributions of all the component terms of the His are statistically different from CLE and from MTFR at the 5% level in both models by using a two-sample Kolmogorov-Smirnov test, while the distributions in CLE and MTFR are significantly different in HadGEM3-GC2 only, consistent with our conclusion based on the bootstrapping approach. The changes of the three components of HWI demonstrate the atmospheric conditions favoring haze events all become more likely with global warming, and that future AA reductions may further increase their likelihood.

4.2 Possible mechanism for atmospheric circulation changes

Section 4.1 showed that the projected change of mean state of the large-scale atmospheric circulation in the future will increase the frequency of circulation patterns currently associated with Beijing haze events. Rapid reductions in AA emissions could cause a further increase. To investigate the mechanism underlying these circulation changes, we present the spatial patterns of the changes in the vertical temperature profile, and 850-hPa and 500-hPa winds in Figs.5-7. The lower- and mid-troposphere displays an incremental warming from His to MTFR compared to the upper levels in both models. The peak warming is at 700 hPa and over 120°-130°E. Conversely, both models simulate an upper-tropospheric cooling at 250 hPa in CLE compared to His,

Deleted: The shift in the HWI distributions shown in Fig. 3c-d is also associated with increase in atmospheric circulation patterns currently associated with the most severe haze events. Very extreme events (HWI ≥ 3) in HadGEM3-GC2 account for only 0.3% of the total historical events. This almost doubles in CLE, and increases by a factor of 5 in MTFR. This kind of event never happened in the current baseline of GFDL-CM3, but accounts for about 0.3% of events in MTFR. This change indicates that both greenhouse gas increases and aerosol reductions may increase the frequency of occurrence of the atmospheric circulation pattern currently associated with severe haze events over the Beijing region.

Formatted: Font color: R,G,B (4,50,255)

Formatted: Font:12 pt

Formatted: Font color: R,G,B (4,50,255)

Deleted: 4

Formatted: Font color: R,G,B (4,50,255)

Deleted: This shift is mainly caused by the increase in the mean values of ΔT, U500 and V850. In both models,

Deleted: t

Deleted: between His and

Deleted: (

Formatted: Font color: R,G,B (4,50,255)

Formatted: Font color: R,G,B (4,50,255)

Deleted:). As for HWI, the distributions of the three component terms are significantly different between CLE and MTFR in HadGEM3-GC2, but not GFDL-CM3

Deleted: For HadGEM3-GC2 (GFDL-CM3), the frequencies of ΔT≥1, U500≥1 and V850≥1 have increased from 14.0%, 17.0%, and 7.2% (16.7%, 18.0%, and 17.8%) in His to 29.3%, 26.8%, and 16.0% (30.2%, 25.1%, and 22.2%) in CLE, and to 37.2%, 36.3%, and 22.7% (25.8%, 32.7%, and ... [12]

Formatted: Indent: First line: 0 ch

albeit of smaller magnitude than the warming below (Fig.S7). However, the 250 hPa temperature changes between MTFR and CLE differ in the two models (Fig.5b, d and Fig.S7g-h). Thus, the increase in tropospheric stability in MTFR relative to CLE is mainly driven by low-level warming.

Following the CLE aerosol pathway, both HadGEM3-GC2 and GFDL-CM3 project an anomalous 850-hPa cyclonic circulation over the northwestern Pacific (0-20°N, 120-180°E) relative to His, and an anticyclonic anomaly to its north (20-50°N, 120-180°E) (Fig.6a-b). This pattern bears some resemblance to the anomalous circulation associated with a positive phase of the Arctic Oscillation, which may be due to melting Arctic sea ice (Shindell et al. 1999; Fyfe et al. 1999; Chen et al. 2017; Wang et al. 2017). The southerly wind anomalies over eastern China, on the western flank of the anomalous anticyclone, act to weaken the East Asian winter monsoon and reduce its low-level winds, making conditions favorable for air-pollutant transport from south to north and air-pollutant accumulation more likely. With the addition of rapid AA reductions following MTFR, the 850-hPa circulation anomalies are reinforced further (Fig6.c-d), especially in HadGEM3-GC2, which simulates much stronger southerly wind anomalies along the East Asian coast. GFDL-CM3 shows similar anomalies over the North Pacific in CLE vs. His and MTFR vs. His, but distinct responses over China (Fig.6d), which likely explains why GFDL-CM3 doesn't simulate the further shift in HWI seen in HadGEM3-GC2 between CLE and MTFR (Fig.S6c, f). A northeasterly anomaly is seen over southeast China in GFDL-CM3 in both CLE relative to His and

Deleted: 5
Deleted: a-b, e-f
Formatted: Font color: R,G,B (4,50,255)
Formatted: Font color: R,G,B (4,50,255), Not Highlight
Formatted: Not Highlight
Formatted: Font color: R,G,B (4,50,255)
Deleted: 5
Deleted: c-d,
Deleted: CLE
Deleted: 4e
Deleted: and Table S2

MTFR relative to CLE. However, the onshore flow over Beijing seen in CLE relative to His, which is likely to be a key contributor to an increase in haze weather events, is not enhanced further by the rapid aerosol reductions in MTFR (Fig. 6d).

At 500 hPa, a northward shift of the westerly jet stream is projected in CLE relative to the current baseline, with significant positive zonal wind anomalies along 50°N and negative anomalies along 30°N in both models (Fig.7a-b). This shift is consistent with the increase in the meridional temperature gradient over the North Pacific (Fig. S7). Thus, the East Asian winter trough is weakened, bringing less cold and dry air to the Beijing area, and favoring the formation and maintenance of haze events. The reductions in AA emissions in MTFR relative to CLE significantly strengthen the above-mentioned circulation anomalies at 500 hPa in both models (Fig 7c,d), and further increase the frequency of positive U500 differences in the regions used to calculate the HWI, as seen in Fig. 7c-d. The changes in 500-hPa zonal winds are consistent between the two models, demonstrating the robustness of the results.

Deleted: S5

Deleted: and Table S2

The changes in the three components of HWI in CLE relative to His indicate a weakened EAWM with increased GHGs, with reductions in AA emissions further amplifying this effect and increasing the frequency of large-scale circulation conditions conducive to Beijing haze events. To explore how the EAWM circulation responds to reductions in AA emissions, we show surface temperature and sea level pressure changes in MTFR relative to CLE (Fig. 8). Reduced AA emissions generally amplify the impact of greenhouse gases, with more warming over the Arctic, the Eurasian continent and Northwestern Pacific. Thus, the Aleutian low is further weakened in MTFR. In addition, more warming over the Eurasian continent and Northwestern Pacific leads to a SLP decrease over Siberia and the northwestern Pacific, respectively. The main difference between the two models is found from the SLP changes over the Eurasian continent in the mid-latitudes, where large negative SLP anomalies are presented in HadGEM3-GC2 while there are no changes in GFDL-CM3. This may lead to the less westward shift of the North Pacific anomalous anticyclonic circulation in GFDL-CM3 in Fig.6d.

The PDF distributions of EAWM, using the Wang and Chen (2014) index, in His, CLE and MTFR are shown in Fig.8e-f. The EAWM weakens in CLE compared to His (blue and grey lines in Fig.8e-f), mainly due to increased SLP over the North Pacific (SLP_2, Fig.S8 b, e), with no systematic changes in SLP over Siberia (SLP_1) and the Maritime continent (SLP_3) (Fig.S8a,d, and Fig.S8c,f). The rapid AA reductions in MTFR cause the SLP over Siberia to decrease consistently in both models alongside a increase in SLP_2. The changes in SLP_2 (SLP_1) are statistically significant at the 5% (10%) level in both models tested by performing bootstrapped samples (not shown). This further weakens the east-west contrast, leading to a weaker EAWM in MTFR relative to CLE, consistent with the differences between CLE and His and between MTFR and CLE seen in the HWI. The response of SLP over the Maritime Continent (SLP_3) to AA reductions differs between the two models, indicating large uncertainty in the SLP_3 changes. Thus, the AA forcing reduction predominantly weakens the EAWM through

Deleted: Histograms
Formatted: Font color: R,G,B (4,50,255)
Deleted: and its components
Formatted: Font color: R,G,B (4,50,255)
Deleted: 9
Formatted: Font color: R,G,B (4,50,255)
Deleted: 9
Deleted: a
Deleted: b
Formatted: Font color: R,G,B (4,50,255)
Formatted: Font color: R,G,B (4,50,255)
Deleted: 9
Deleted: e
Deleted: -
Deleted: f
Formatted: Font color: R,G,B (4,50,255)
Deleted: 9
Formatted: Font color: R,G,B (4,50,255)
Deleted: -b
Formatted: Font color: R,G,B (4,50,255)
Deleted: h-
Deleted: g
Formatted: Font color: R,G,B (4,50,255)
Deleted:
Deleted: n
Formatted: Font color: R,G,B (4,50,255), Not Highlight
Deleted: increase
Formatted: Font color: R,G,B (4,50,255)
Formatted: Font color: R,G,B (4,50,255), Not Highlight
Deleted: ,
Formatted: Font color: Red

reducing the zonal thermal contrast.

4.3 Changes in haze intensity associated with favoring circulation

Occurrence of a haze event requires stagnant atmospheric conditions, and also a pollution source. Although future aerosol reductions may cause further increases in the frequency of atmospheric circulation patterns currently linked with haze events, such events may be less severe in the absence of large aerosol emissions. In this section, we will examine the projected changes in the intensity of Beijing haze events using the aerosol optical depth (AOD) at 550nm as a metric for aerosol-induced poor visibility. The simulated baseline winter mean AOD around Beijing area is about 0.1 (Fig.9a, c). To account for model differences in historical AOD, we used the ratio of AOD at 550nm (hereafter AOD_ratio) relative to a baseline winter mean to represent the air-pollution severity. When AOD_ratio is greater than 1.0, the air-pollution intensity is higher than baseline climate mean. HadGEM3-GC2 and GFDL-CM3 both simulate elevated AOD around Beijing when circulation conditions are favorable (HWI≥1) (Fig.9 b, d): 1.4 and 1.3 times of the baseline climate mean in HadGEM3-GC2 and GFDL-CM3 respectively. Aerosol and precursor emission increases under CLE (Fig. S1) result in a significant increase in climate winter mean AOD around Beijing (reaching 1.2 times in HadGEM3-GC2 and 1.05 times in GFDL-CM3), while climate mean AOD in MTFR decreases to 0.93 of the baseline climate mean around Beijing in the two models due to aerosol emissions reduction (Fig.S9).

To check whether poor air quality events still occur even with reduced future aerosol

Formatted: Indent: First line: 0 ch

Deleted: in the

Deleted: around

Deleted: 10a

Deleted: 10

Deleted: S6

Formatted: Font color: R,G,B (4,50,255)

emissions, we show the projected AOD_ratio with HWI≥1 in Fig.10. In CLE, when HWI≥1, AOD_ratio is elevated compared to the baseline climatology, to 1.6 times of the baseline winter mean in HadGEM3-GC2 and 1.1 times that in GFDL-CM3 (Fig.10a, c). It is consistent with the increase in aerosol loadings and climate mean AOD in CLE (Fig.S2a and Fig.S9a-b). However, in MTFR, when HWI≥1 AOD is also higher than the baseline climatology, albeit with a decrease in climate mean AOD in MTFR (Fig.10 b,d). So, even with the aggressive aerosol reductions in MTFR, periods of poor visibility still occur in conjunction with atmospheric circulation patterns associated with haze in the current climate.

We calculated the PDF distributions of AOD_ratio surrounding the Beijing region (box region in Fig.2) in the months with HWI≥1 in His, CLE and MTFR (Fig.11). In His, the area-averaged AOD_ratio around the Beijing region when HWI≥1 is elevated to 1.34 (1.26) times of the baseline climate mean in HadGEM-GC2 (GFDL-CM3) (Fig11.a-b). The change in AOD_ratio with HWI≥1 under CLE relative to His is different between the two models. It increases to 1.51 in HadGEM3-GC2 but decreases to 1.13 in GFDL-GC3. As expected, the AOD_ratio with HWI≥1 in MTFR reduces in both models due to the dramatic reduction in anthropogenic aerosols. Thus, the mean air-pollution intensity with the favorable circulation conditions for haze under MTFR will be greatly relieved.

This reduction in GFDL-CM3 in CLE relative to His may be a reflection of the model's bias. In JRA-55 when HWI≥1 there are southerly anomalies over southern China.

Deleted: as a fraction of the baseline winter mean
Formatted: Font color: R,G,B (4,50,255)
Deleted: 11
Deleted: (Fig. 11)
Formatted: Highlight
Formatted: Highlight
Deleted: S1a
Deleted: S6a
Deleted: S6c
Deleted: -

Deleted: The severity of air quality under the circulation patterns favoring haze (when HWI≥1) changes differently between CLE and MTFR. Thus, we compared months when HWI≥1 shows the effect of aerosol emission changes on haze intensity under the same circulation patterns (Fig. 12). For HWI≥1, AOD over Beijing is comparable in CLE to His in HadGEM3-GC2, but slightly reduced in GFDL-CM3, despite the increase in aerosol emissions.
Formatted: Font color: R,G,B (4,50,255)

However, in the baseline in GFDL-CM3 there is an anomalous cyclonic circulation, which may act to reduce pollutant accumulation in Beijing (Fig.S5). As shown in Fig. 6b, d, this anomaly is strengthened in both CLE and MTFR.

To check whether extreme air pollution events would still occur, the probability of AOD_ratio when HWI≥1 in the three scenarios are examined (Fig.11b, d). In this study, the mean AOD_ratio across all months when HWI≥1 in His is regarded as the winter mean intensity of baseline haze events, i.e., the grey vertical lines in Fig.11a, c. The probability of haze event intensity exceeding this threshold is about 42% and 34% in HadGEM3-GC2 and GFDL-CM3, respectively (Fig.11b, d). Under CLE, it increases to 52% in HadGEM3-GC2 while decreases to 28% in GFDL-CM3, consistent with Fig.10a, c. In MTFR, lower probability is projected in both models, 24% in HadGEM-GC2, and 21% in GFDL-CM3. This demonstrates that severe events (i.e., higher AOD_ratio) would still happen in MTFR albeit with dramatic reduction in anthropogenic aerosol, even though the mean intensity of haze events themselves will become less dangerous if aerosol emissions are reduced.

5 Summary and discussion

During recent decades, with rapid increases in aerosol and precursor emissions in China, air pollution has become one of the greatest threats to public health. Anthropogenic aerosol contributes not only to the chemical composition of haze, but also has the potential to modulate atmospheric circulation changes. Thus, this paper aims to quantify the incidences of haze events in a future climate and the influence of aerosol

Deleted: 4

Formatted: Not Highlight

Deleted: When HWI≥1 in MTFR, both models show a significant reduction in AOD compared to baseline events when HWI≥1.

Deleted: This demonstrates that the air quality is similar under CLE to the baseline condition under the favorable circulation patterns of haze, but it is much improved under MTFR (Fig.12e-f).

Summary and

Formatted: Font color: R,G,B (4,50,255)

Deleted: A higher criterion for HWI value may be better to examine the projected changes in haze events if aerosol emissions are reduced.

Formatted: Indent: First line: 0 ch

mitigation efforts. In this study, we examined the changes in the frequency of atmospheric conditions conducive to Beijing haze events, and the changes in aerosol optical depth (AOD) during these circulation conditions through the mid-21st century under two different anthropogenic aerosol scenarios. We also investigated the mechanism for the changes in the large-scale atmospheric circulation.

We found that future greenhouse gases (GHG) increases and anthropogenic aerosol (AA) increases following a current legislation aerosol scenario (CLE) will increase the frequency of haze-favorable atmospheric circulation conditions surrounding the Beijing region. The frequency of haze weather index (HWI)≥1 derived from monthly data in HadGEM3-GC2 (GFDL-GCM3) increases from ~18% (16%) at baseline to ~28% (31%) for 2016-2050 under the CLE scenario. By comparing the scenario with a maximum technically feasible aerosol reduction (MTFR), which has the same GHG increases but rapid aerosol reductions, we show that future aerosol reductions may further amplify the increase in the frequency of such circulation patterns. Rapid reductions in AA emissions in MTFR contribute to an extra ~6% increase in HWI≥1 in two models.

The increase in haze frequency in CLE is mainly due to a weakening of the East Asian winter monsoon, warming of the lower troposphere, and weakening of the East Asian trough, which is likely to be predominantly driven by the GHG increases. Reduced AA forcing in MTFR could further enhance the above circulation anomalies, amplifying the impact of greenhouse gases. Because the AA emission reductions in MTFR relative

Deleted: atmospheric circulation conditions conducive to Beijing haze events, especially the very extreme circulation patterns

Deleted: The frequency of haze weather index (HWI)≥1.0 derived from monthly data increases from ~16% at baseline to ~28% for 2016-2049 under the CLE scenario.

Formatted: Font color: R,G,B (4,50,255)

Deleted: 7

Deleted: : HadGEM3-GC2 and GFDL-CM3

Deleted: We also find that the frequency of exceptional extreme circulation events with HWI≥3.0 in HadGEM3-GC2 is only 0.3% in His, but is almost doubled in CLE and increases by a factor of 5 in MTFR. These kinds of events never happen in the baseline in GFDL-CM3, but account for 0.3% of events in MTFR.

to CLE mainly occur over continental Asia, the Asian landmass receives more shortwave radiation, leading to a warmer surface temperature there. This leads to a weaker Siberian high, and further contributes to the weakening of the East Asian winter monsoon in MTFR.

The analysis of haze intensity based on AOD at 550 nm shows that visibility with HWI≥1.0 is always lower than the His winter mean under both CLE and MTFR. With more reduction in aerosol emissions following the MTFR, the mean intensity of haze events in the haze-favorable atmospheric circulation will become less dangerous compared to that in His and CLE in both models. Meanwhile, the probability of haze event with intensity exceeding the baseline mean also decrease in MTFR, demonstrating that severe haze events would also occur in MTFR.

This paper reveals the competing impacts of AA emission reductions on haze event frequency and intensity. AA reductions cause an increased frequency of atmospheric circulation patterns conducive to haze events, but a reduction in the haze intensity when these circulation patterns do occur. We found that the capability of the models in representing haze-favorable large-scale circulations may impact the simulation of AOD, which introduces further uncertainties in future projection of AOD. Model evaluation on haze-favorable circulation and associated AOD is necessary for future projection. Our results are consistent with previous studies that global warming, and more reduction in aerosol forcing caused extra warming, will make haze-favorable conditions around Beijing area more frequent (Callahan and Markin, 2020). But internal variability

Deleted: seen

Deleted: However, i

Formatted: Font color: R,G,B (4,50,255)

Deleted: n future the haze events associated with HWI≥1.0 are comparable, or less severe, than their baseline equivalents. Under MTFR, there is a marked reduction in the AOD associated with HWI≥1.0 compared to His. This demonstrates that even though the atmospheric circulations that favor haze events will become more frequent as GHG increases and AA decreases, the haze events themselves will become less dangerous if aerosol emissions are reduced.

Formatted: Font color: R,G,B (4,50,255)

Deleted:

Formatted: Font color: R,G,B (4,50,255)

may not be fully sampled because of limited number of realization and models used in this study. In the future, single forcing experiments and large ensemble simulations are useful ways to confirm the relative role of greenhouse gases and anthropogenic aerosol forcing on haze events.

Code/Data availability: The National Climatic Data Center (NCDC) Global Surface Summary of the Day (GSOD) database can be downloaded from the GSOD website (https://catalog.data.gov/dataset/global-surface-summary-of-the-day-gsod). The JRA-55 reanalysis data can be freely downloaded from the rda.ucar.edu website (https://rda.ucar.edu/datasets/ds628.0/). Requests for outputs of the His, CLE and MTFR experiments, or any questions regarding the data, can be directed to the corresponding author, L Zhang (lixiazhang@mail.iap.ac.cn).

Deleted: This demonstrates that the local air quality benefits from clean air policies outweigh the dynamical climate impact of aerosol and precursor emission reductions in this case.

Formatted: Font color: R,G,B (4,50,255)

Author contribution: L Zhang designed and wrote the manuscript with support from all authors. LJW and MAB helped design the analysis and supervised the work. NJD and DJP ran the simulations. Shuai Hu analyzed the reanalysis data. Donghuan Li and Liwei Zou contributed to the validation of observational metrics.

Competing interests: The authors declare that they have no conflict of interest.

Acknowledgement: This work was jointly supported by the Ministry of Science and Technology of China under Grant 2018YFA0606501 and the National Natural Science Foundation of China under grant No. 41675076. LJW, MAB and JKPS were supported by the UK-China Research & Innovation Partnership Fund through the Met Office Climate Science for Service Partnership (CSSP) China as part of the Newton Fund.

Liwei Zou is supported by National Natural Science Foundation of China under grant No. 41830966.

Reference:

Amann M., I. Bertok, J. Borken-Kleefeld, J. Cofala, C. Heyes, L. Hoglund-Isaksson, G. Kiesewetter, Z. Klimont, W. Schöpp, N. Vellinga, W. Winiwarter: Adjusted historic emission data, projections, and optimized emission reduction targets for 2030 – A comparison with COM data 2013. Part A: Results for EU-28. TSAP Report #16A, version 1.1. IIASA, Laxenburg, Austria, 2015.

An Z., R. Huang, R. Zhang, X. Tie, G. Li, J. Cao, W. Zhou, Z. Shi, Y. Han, Z. Gu, Y. Ji: Severe haze in northern China: A synergy of anthropogenic emissions and atmospheric processes. Proceedings of the National Academy of Sciences of the United States of America, 116 (18): 8657–8666, https://doi.org/10.1073/pnas.1900125116, 2019.

Cai W J, K. Li, H. Liao, H. Wang, L. Wu: Weather conditions conducive to Beijing severe haze more frequent under climate change, Nat. Clim. Change. 7: 257–62, 2017.

Callahan, C. W., & Mankin, J. S.: The influence of internal climate variability on projections of synoptically driven Beijing haze. Geophysical Research Letters, 46, e2020GL088548. https://doi.org/10.1029/2020GL088548, 2020.

Formatted: Font color: Text 1

Formatted: Font color: Text 1

Formatted: Font color: Text 1

Callahan, C. W., Schnell, J. L., and Horton, D. E.: Multi-index attribution of extreme winter air quality in Beijing, China. Journal of Geophysical Research: Atmospheres, 124, 4567–4583. https://doi.org/10.1029/2018JD029738, 2019.

Chakravarti, Laha, and Roy, 1967: Handbook of Methods of Applied Statistics, Volume I, John Wiley and Sons, pp. 392-394.

Chen, H.P., H. J., Wang: Haze Days in North China and the associated atmospheric circulations based on daily visibility data from 1960 to 2012. J. Geophys. Res. Atmos. 120, 5895–5909, https://doi.org/10.1002/2015JD023225, 2015.

Chen H., H. Wang, J. Sun,Y. Xu, Z. Yin: Anthropogenic fine particulate matter pollution will be exacerbated in eastern China due to 21st century GHG warming. Atmospheric Chemistry and Physics, 19, 233–243, https://doi.org/10.5194/acp-19-233-2019, 2019.

China State Council: Action Plan on Prevention and Control of Air Pollution, China State Council, Beijing, China, http://www.gov.cn/zwgk/2013-09/12/content_2486773.htm (last access: 17 January 2021), 2013.

Ding, Y. H. and Liu, Y. J.: Analysis of long-term variations of fog and haze in China in recent 50 years and their relations with atmospheric humidity, Sci. China Earth Sci., 57, 36–46, 2014.

Donner, L. J., B. L. Wyman, R. S. Hemler, L. W. Horowitz, Y. Ming et al.: The dynamical core, physical parameterizations, and basic simulation characteristics

Formatted: Font color: R,G,B (4,50,255)

Formatted: Font color: R,G,B (4,50,255)

Formatted: Indent: Left: 0 cm, Hanging: 0.85 cm, Space Before: 0 pt, Line spacing: single

Formatted: Font color: Text 1

Deleted:

of the atmospheric component of the GFDL global coupled model CM3. Journal of Climate, 24, 3484–3519, DOI: 10.1175/2011JCLI3955.1 2011.

Feng J., J. Quan, H. Liao, Y. Li and X. Zhao: An Air Stagnation Index to Qualify Extreme Haze Events in Northern China. Journal of the Atmospheric Sciences, 75, 3489-3505. doi:10.1175/JAS-D-17-0354.1. 2018.

Fyfe, J. C., Boer, G. J. and Flato, G. M.: The Arctic and Antarctic oscillations and their projected changes under global warming. Journal of Geophysical Research, 26, 1601–1604, 1999.

Griffies S., M. Winton, L. Donner, et al.: The GFDL CM3 Coupled Climate Model: Characteristics of the Ocean and Sea Ice Simulations. Journal of Climate, 24(13), 3520-3544, 2011.

Han Z., B. Zhou, Y. Xu, J. Wu and Y. Shi: Projected changes in haze pollution potential in China: an ensemble of regional climate model simulations. Atmospheric Chemistry and Physics, 17, 10109–10123. https://doi.org/10.5194/acp-17-10109-2017, 2017.

He J., Gong S., Zhou C. et al.: Analyses of winter circulation types and their impacts on haze pollution in Beijing. Atmospheric Environment, 192, 94–103, 2018.

Hori, M.E. and Ueda, H.: Impact of global warming on the East Asian winter monsoon as revealed by nine coupled atmosphere-ocean GCMs. Geophysical Research Letters, 33(3): L03713, 2006.

Deleted:

Formatted: First line: -2 ch

Deleted: Francis JA, Vavrus S J.: Evidence linking Arctic amplification to extreme weather in mid-latitudes. Geophysical Research Letters, 39, 06801, 2012. Griffies S., M. Winton, L. Donner, et al.: The GFDL CM3

Formatted: Font color: Text 1

Kobayashi, S., and Coauthors: The JRA-55 reanalysis: general specifications and basic characteristics. Journal of the Meteorological Society of Japan, 93(1), 5-48,doi:http://doi.org/10.2151/jmsj.2015-001, 2015.

Jeong Jaein I., and Rokjin J. Park: Winter monsoon variability and its impact on aerosol concentrations in East Asia. Environmental Pollution, 221, 285e292, 2017.

Lamarque J, Bond T, Eyring V, et al.: Historical (1850-2000) gridded anthropogenic and biomass burning emissions of reactive gases and aerosols: Methodology and application, Atmospheric Chemistry and Physics, 10: 7017−7039, 2010.

Li, Q., Zhang, R., Wang, Y.: Interannual variation of the wintertime fog-haze days across central and eastern China and its relation with East Asian winter monsoon. International Journal of Climatology. 36, 346e354, 2016.

Li, K., Liao, H., Cai, W., & Yang, Y.: Attribution of anthropogenic influence on atmospheric patterns conducive to recent most severe haze over eastern China. Geophysical Research Letters, 45, 2072–2081. https://doi.org/10.1002/2017GL076570, 2018.

Liu, C., Zhang, F., Miao, L., Lei, Y. & Yang, Q. Future haze events in Beijing, China: When climate warms by 1.5 and 2.0C. Int. J. Climatol. 40, 3689–3700, 2019a.

Liu, Z. et al. A Model Investigation of Aerosol Induced Changes in the East Asian Winter Monsoon. Geophys. Res. Lett. 46, 10186–10195, 2019b.

Formatted: Font color: R,G,B (4,50,255)

Formatted: Font color: R,G,B (4,50,255)

Formatted: Font color: R,G,B (4,50,255)

Luo F., L. Wilcox, B. Dong et al.: Projected near-term changes of temperature extremes in Europe and China under different aerosol emissions. Environmental Research Letters, 15,034013, 2020.

Ming Y., V. Ramaswamy, L. J. Donner, and V. T. J. Phillips: A robust parameterization of cloud droplet activation. J. Atmos. Sci., 63, 1348–1356, 2006.

Niu F., Z. Q. Li, C. Li, K.-H. Lee, and M. Y. Wang: Increase of wintertime fog in China: Potential impacts of weakening of the eastern Asian monsoon circulation and increasing aerosol loading, J. Geophys. Res., 115, D00K20, doi:10.1029/2009JD013484, 2010.

Pei L. and Z. W., Yan: Diminishing clear winter skies in Beijing towards a possible future. Environmental Research Letters, 13,124029, 2018.

Pei L., Z.W, Yan, Z. Sun, S. Miao, Y. Yao: Increasing persistent haze in Beijing: potential impacts of weakening East Asian winter monsoons associated with northwestern Pacific sea surface temperature trends. Atmospheric Chemistry and Physics, 18,3173–83, 2018.

Pei L., Yan Z.W., Chen D., and Miao S.: Climate variability or anthropogenic emissions: which caused Beijing Haze? Environmental Research Letters, 15 034004, 2020.

Scannell, C., and Coauthors: The Influence of Remote Aerosol Forcing from Industrialized Economies on the Future Evolution of East and West African Rainfall. Journal of Climate, 32, 8335–8354, https://doi.org/10.1175/JCLI-D-18-0716.1. 2019.

Formatted: Indent: Left: 0 cm, Hanging: 0.85 cm, Space Before: 0 pt, Line spacing: single

Formatted: Font color: Text 1

Shindell, D. T., R. L. Miller, G. A. Schmidt, L. Pandolfo: Simulation of recent northern winter climate trends by greenhouse-gas forcing. Nature, 399, 452–455, 1999.

Taylor K. E., Stouffer B. J., and Meehl, G. A.: An overview of CMIP5 and the experiment design, Bull. Am. Meteorol. Soc., 93, 485–498, 2012.

Wang, H. J., H. P. Chen, and J. P. Liu: Arctic sea ice decline intensified haze pollution in eastern China, Atmospheric and Oceanic Science Letters, 1–9, 2015.

Wang L., Chen W.: An intensity index for the east Asian winter monsoon. Journal of Climate, 27, 2361. https://dx.doi.org/10.1175/JCLI-D-13-00086.1, 2014.

Wang Y., T. Le, G. Chen, et al.: Reduced European aerosol emissions suppress winter extremes over northern Eurasia. Nature Climate Change,10, 225–230, 2020.

Williams K. D., C. M. Harris, A. Bodas-Salcedo, et al.: The Met office global coupled model 2.0 (GC2) configuration Geoscientific Model Development, 8,1509–24, 2015.

Wu P., Y. Ding, Y. Liu: Atmospheric circulation and dynamic mechanism for persistent haze events in the Beijing–Tianjin–Hebei region. Advances in Atmospheric Sciences, 34, 429–40, doi: 10.1007/s00376-016-6158-z. 2017.

Zhang, R.H., Li, Q., Zhang, R.N.: Meteorological conditions for the persistent severe fog and haze event over eastern China in January. Science China Earth Sciences, 57, 26–35. https://doi.org/10.1007/s11430-013-4774-3, 2014.

Deleted: Screen JA, Simmonds I.: The central role of diminishing sea ice in recent Arctic temperature amplification. Nature, 464, 1334–1337, 2010.

Formatted: Indent: Left: 0 cm, Hanging: 0.85 cm, Space Before: 0 pt, Line spacing: single

Formatted: Font color: Text 1

Deleted: Wang J., W. Qu, C. Li et al.: Spatial distribution of wintertime air pollution in major cities over eastern China: Relationship with the evolution of trough, ridge and synoptic system over East Asia. Atmospheric Research. 212, 186-201, 2018.

Formatted: Indent: Left: 0 cm, Hanging: 0.85 cm, Space Before: 0 pt, Line spacing: single

Formatted: Font color: Text 1

Deleted: Wilcox L., N. Dunstone, A. Lewinschal, M. Bollasina, A. Ekman, E. Highwood: Mechanisms for a remote response to Asian aerosol emissions in boreal winter. Atmospheric Chemistry and Physics, 19, 9081–95, 2019.

Deleted: Zhang, L., Liao, H., Li, J.: Impacts of Asian summer monsoon on seasonal and interannual variations of aerosols over eastern China. Journal of Geophysical Research: Atmospheres. 115, 2010.

Zhang Y.J., Yin Z.C., Wang H.J.: Roles of climate variability on the rapid increases of early winter haze pollution in North China after 2010. Atmos. Chem. Phys., 20, 12211–12221, 2020.

Zheng B., D. Tong, M. Li, et al: Trends in China's anthropogenic emissions since 2010 as the consequence of clean air actions. Atmospheric Chemistry and Physics, 18, 14095–111, 2018.

Formatted: Font color: R,G,B (4,50,255)

Figure Captions:

Fig. 1 Composite circulation anomalies from JRA-55 with HWI-daily>0 (left) and HWI-month≥1 (right) for 1958-2013. (a)-(b) temperature anomalies (K) along 40°N, (c)-(d) 500hPa winds anomalies (vector, m s^{-1}) and 500hPa zonal winds anomalies (shading, m s^{-1}). (e)-(f) 850hPa winds anomalies (vector, m s^{-1}) and 850 hPa meridional winds anomalies (shading, m s^{-1}). The green boxes/lines indicate the location of the boxes/lines used in the calculation of HWI.

Fig.2 Changes in winter HWI from 1958 to 2013 in JRA-55 reanalysis relative to 1958-2013 winter mean. (a) DJF mean monthly-based HWI (HWI-month, black line) and the anomalous days with daily based HWI >0 (HWI-daily, red line, unit: day), (b) scatter plot of HWI-month of the monthly values from December, January and February (y-axis) and HWI-daily averaged in the same month as HWI-month (x-axis). (c)-(d) are the anomalies of haze occurrence and the VN3day when HWI≥1, where VN3day is the minimum 3-day consecutive visibility. Cross area in (c)-(d) is statistically significant at the 10% level using a Student's t-test.

Fig.3 (a) Probability density function (PDF) via a non-parametric density estimation, Kernel density estimation, and (b) cumulative distribution function (CDF) distributions of HWI in winters of His (1980-2004, grey), CLE (2016-2050, blue) and MTFR (2016-2050, pink) simulated by HadGEM3-GC2. (c)-(d) are results for GFDL-CM3. The numbers in (a) and (c) are the climate mean of HWI, and in (b) and (d) are the frequency of month with HWI≥1, respectively.

Deleted: **Table 1** Frequency (unit: %) of different HWI bins in His, CLE and MTFR

Formatted: First line: -2 ch

Deleted: .0

Deleted: /

Formatted: Superscript

Deleted: (c) same as (a), but for HWI-month (y-axis) and the ratio of days with HWI-daily>0 (x-axis) in each winter month. HWI-month and HWI-daily are the HWI calculated from monthly data and daily data, respectively.

Formatted: Font color: Text 1

Fig.4 (a) Probability density function (PDF) via a non-parametric density estimation, Kernel density estimation, and (b) cumulative distribution function (CDF) distributions of HWI in winters of His (1980-2004, grey), CLE (2016-2050, blue) and MTFR (2016-2050, pink) simulated by HadGEM3-GC2. (c)-(d) are results for GFDL-CM3. The numbers in (a) and (c) are the climate mean of HWI, and in (b) and (d) are the frequency of month with HWI≥1, respectively.

Fig.4 Histogram plots for the 2000 bootstrapped samples of (a) changes in winter mean HWI, and (b) frequency with HWI≥1 in HadGEM3-GC2, and (c)-(d) similarly for GFDL-CM3. The grey, blue and pink shadings are the results estimated from His, CLE and MTFR respectively. Solid (dashed) grey, blue and pink lines are the results of multi-member mean (95% confidence level) in His, CLE and MTFR, respectively.

Fig.5 The difference in winter mean temperature (K) along 40°N (left) between CLE (2016-2050) and His (1980-2004), and (right) between MTFR (2016-2050) and CLE (2016-2050). The dotted areas are statistically significant at the 10% level using a Student's t-test. The green lines indicate the level and longitude used in the calculation of ΔT.

Fig.6 Spatial distribution for the difference in 850 hPa winds (vector, m s^{-1}) and 850hPa meridional component (shading, m s^{-1}) between (left) CLE (2016-2050) minus historical (1980-2004), and between (right) MTFR (2016-2049) minus CLE (2016-2050). The dotted areas denote the 850hPa meridional winds statistically

Deleted: 3

Deleted: Changes in HWI in His (grey line), CLE (blue) and MTFR (pink) experiments simulated by (a) HadGEM3-GC2 and (b) GFDL-CM3 for the winters from 1965 to 2049.

Deleted: Histogram plots for HWI frequency (y-axis, %) simulated by (c) HadGEM3-GC2 and (d) GFDL-CM3. The x-axis in (c)-(d) shows different bins of HWI, and grey, blue and pink bars are for His (1980-2004), CLE (2016-2049) and MTFR (2016-2049), respectively.

Deleted: Same as Fig.3c-d, but for the histograms of each component of HWI simulated by HadGEM3-GC2 (left) and GFDL-CM3 (right). (a)-(b) ΔT, (c)-(d) U500 and (e)-(f) V850.

Deleted: 49

Deleted: 2049

Deleted: 49

Deleted: .

Deleted: 49

Deleted: 49

significant at the 10% level using a Student's t-test. The black box indicates the region used in the calculation of V850.

Fig.7 Same as Fig.6, but for the difference in 500hPa winds (vector, m s^{-1}) and its zonal component (shading, m s^{-1}). The black boxes indicate the regions used in the calculation of U500.

Fig.8 The difference of the climate mean surface temperature (left, K) and sea level pressure (right, hPa) between MTFR and CLE simulated by (a)-(b) HadGEM3-GC2 and (c)-(d) GFDL-CM3. The dotted areas in (a)-(d) are statistically significant at the 10% level using a Student's t-test. PDF via Kernel density estimation of EAWM in His (1980-2004, grey), CLE (2016-2050, blue) and MTFR (2016-2050, pink) simulated by (e) HadGEM3-GC2, and (f) GFDL-CM3. The numbers in (e)-(f) are the climate mean of EAWM.

Fig.9 Winter mean (left) AOD at 550 nm in (a) HadGEM3-GC2 and (c) GFDL-CM3 averaged over 1980-2004. Right is same as left, but for the mean AOD_ratio of AOD averaged in the winter months with HWI≥1 (hereafter AOD_ratio(HWI≥1)) in His. Blue and red shadings in (b) and (d) are decreased and elevated AOD relative to the baseline mean, respectively.

Fig.10 Same as Fig.9b and d, but for the results projected in CLE and MTFR. The dotted areas are statistically significant at the 10% level using a Student's t-test.

Fig.11 (a) PDF and (b) CDF distributions of AOD_ratio(HWI≥1) over North China

Deleted: 90% confidence level.

Formatted: Font color: Text 1

Deleted: Same as Fig.4, but for histograms of the East Asian winter monsoon index and its components.

Deleted: DJF mean (left) AOD at 550 nm in (a) HadGEM3-GC2 and (c) GFDL-CM3 averaged over 1980-2004. Right is same as left, but for the ratio of AOD averaged in the winter months with HWI≥1 relative to winter mean of 1980-2004. Blue and red shadings in (c)-(d) are lower and higher than the climate mean of baseline, respectively.

(33-45°N, 105-122°E, box in Fig.2) in HadGEM3-GC2. (c)-(d) are the results from GFDL-CM3. The grey, blue and pink vertical lines and numbers in (a) and (c) are the winter mean AOD_ratio(HWI≥1) of His, CLE and MTFR, respectively. The numbers in (b) and (d) are the cumulative probability of AOD_ratio(HWI≥1) higher than the winter mean AOD_ratio(HWI≥1) of His.

Deleted: Same as Fig.10b and d, but for the results projected in CLE and MTFR. The baseline is the winter mean of 1980-2004.

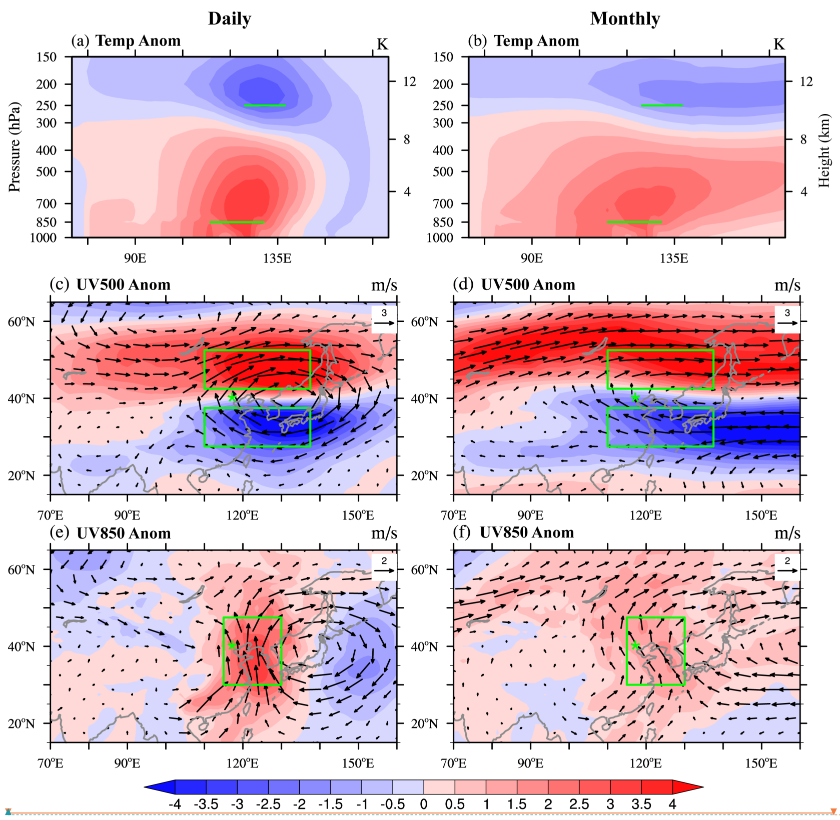

Fig. 1 Composite circulation anomalies from JRA-55 with HWI-daily>0 (left) and HWI-month≥1.0 (right) for 1958-2013. (a)-(b) temperature (K) along 40°N, (c)-(d) 500hPa winds (vector, m s^{-1}) and its zonal component (shading, m s^{-1}). (e)-(f) 850hPa winds (vector, m s^{-1}) and its meridional component (shading, m s^{-1}). The green boxes/lines indicate the regions used to calculate the three components of HWI.

Deleted: **Table 1** Frequency (unit: %) of different HWI bins in His, CLE and

Deleted: MTFR

Exp

... [13]

Formatted: Font:(Default) Times New Roman

Formatted Table

Formatted: Font:(Default) Times New Roman

Deleted: anomalies…(K) along 40°N, (c)-(d) 500hPa winds anomalies

... [14]

Deleted: 500hPa…ts zonal winds …omponent anomalies …shading, m s^{-1}). (e)-(f) 850hPa winds anomalies …vector, m s^{-1}) and 850 hPa…ts meridional winds anomalies…omponent (shading, m s^{-1}). The green boxes/lines indicate the location …egions of the boxes/lines …sed in the…o calculateion…the three components ofof

... [15]

Formatted: Font color: R,G,B (4,50,255)

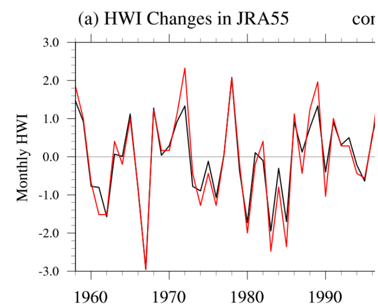

Deleted:

Formatted: Font:(Default) Times New Roman

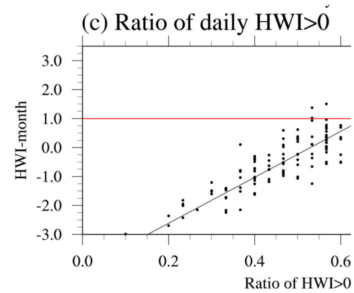

Deleted:

Formatted: Font:(Default) Times New Roman

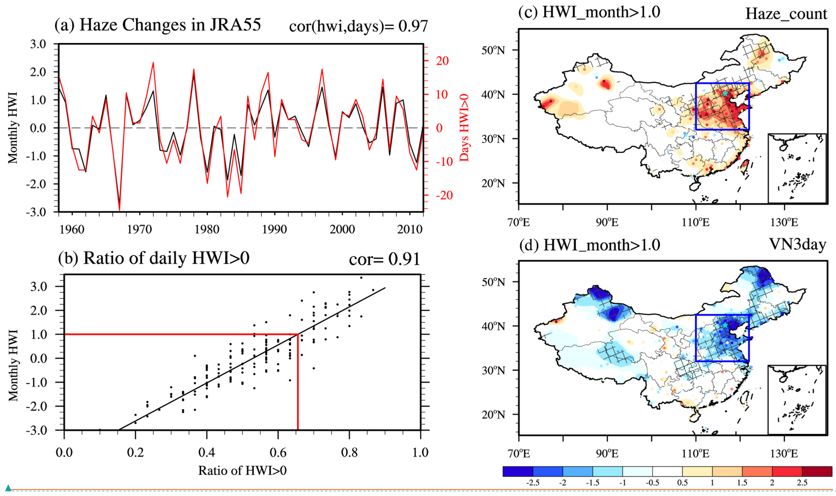

Fig.2 Changes in winter HWI from 1958 to 2013 in JRA-55 reanalysis relative to 1958-2013 winter mean. (a) DJF mean monthly-based HWI (HWI-month, black line) and the anomalous days with daily based HWI >0 (HWI-daily, red line, unit: day), (b) scatter plot of HWI-month of December, January and February (y-axis) and the ratio of days with HWI-daily>0 (x-axis) in each winter month. HWI-month and HWI-daily are the HWI calculated from monthly data and daily data, respectively. (c)-(d) are the anomalies of haze days and the VN3day when HWI≥1, where VN3day is the minimum 3-day consecutive visibility. Cross area in (c)-(d) is statistically significant at the 10% level using a Student's t-test.

Formatted: Font:(Default) Times New Roman

Deleted: the monthly values from

Deleted: HWI-daily averaged in the same month as HWI-month (x-axis). (c) same as (a), but for HWI-month (y-axis) and

Formatted: Font color: R,G,B (4,50,255)

Formatted: Font color: R,G,B (4,50,255)

Deleted:

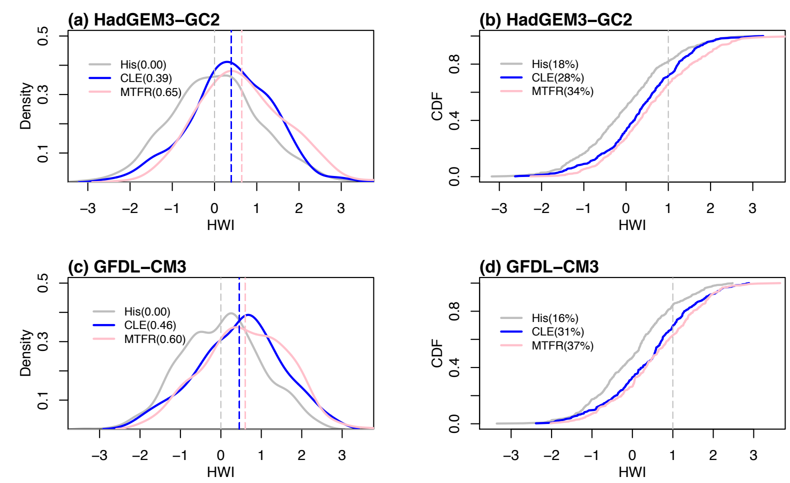

Fig. 3 (a) Probability density function (PDF) via a non-parametric density estimation, Kernel density estimation, and (b) cumulative distribution function (CDF) distributions of HWI in winters of His (1980-2004, grey), CLE (2016-2050, blue) and MTFR (2016-2050, pink) simulated by HadGEM3-GC2. (c)-(d) are results for GFDL-CM3. The numbers in (a) and (c) are the climate mean of HWI, and in (b) and (d) are the frequency of month with HWI≥1, respectively.

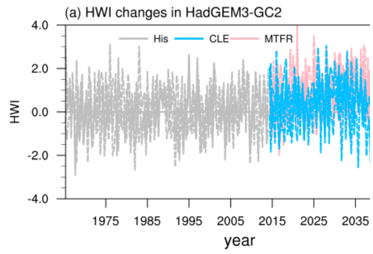

Deleted:

Formatted: Font:(Default) Times New Roman

Formatted: Font:(Default) Times New Roman

Formatted: Widow/Orphan control

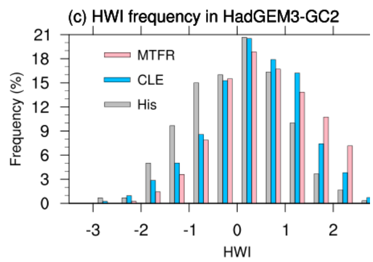

Deleted:

Deleted: 3

Formatted: Font color: R,G,B (4,50,255)

Formatted: Font color: R,G,B (4,50,255)

Deleted: Changes in HWI in His (grey line), CLE (blue) and MTFR (pink) experiments simulated by (a) HadGEM3-GC2 and (b) GFDL-CM3 for the winters from 1965 to 2049. Histogram plots for HWI frequency (y-axis, %)simulated by (c) HadGEM3-GC2 and (d) GFDL-CM3. The x-axis in (c)-(d) shows different bins of HWI, and grey, blue and pink bars are for His (1980-2004), CLE (2016-2049) and MTFR (2016-2049), respectively.

Formatted: Font:(Asian) Times New Roman

Deleted: Page Break

Formatted: Font:(Default) Times New Roman

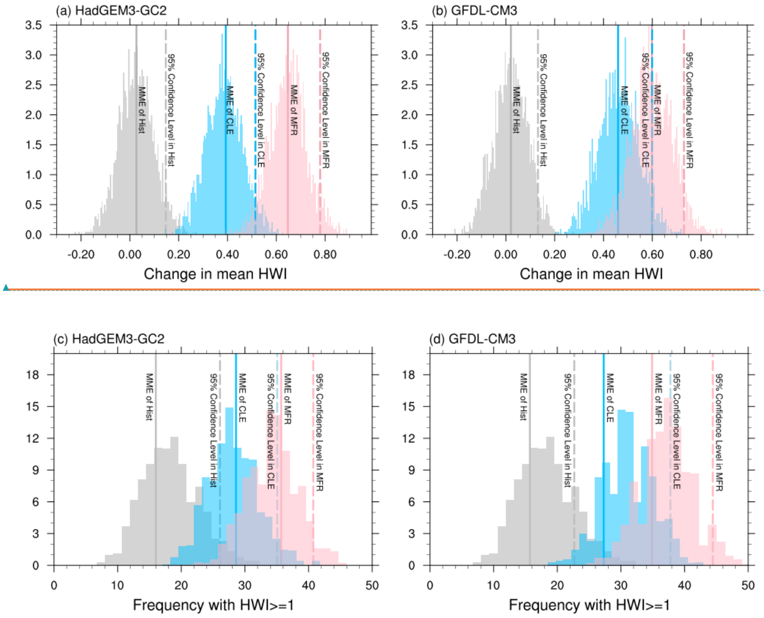

Fig. 4 Histogram plots for the 2000 bootstrapped samples of (a) changes in winter mean HWI, and (c) frequency of month with HWI≥1 in HadGEM3-GC2, and (b), (d) similarly for GFDL-CM3. The grey, blue and pink shadings are the results estimated from His, CLE and MTFR respectively. Solid (dashed) grey, blue and pink lines are the results of multi-member mean (95% confidence level) in His, CLE and MTFR, respectively.

Formatted: Font:(Default) Times New Roman, Bold
Formatted: Line spacing: at least 12 pt
Formatted: Font:(Default) Times New Roman, Bold
Formatted: Font:Bold, Font color: R,G,B (4,50,255)
Formatted: Justified
Formatted: Font color: R,G,B (4,50,255)
Formatted: Font color: R,G,B (4,50,255)

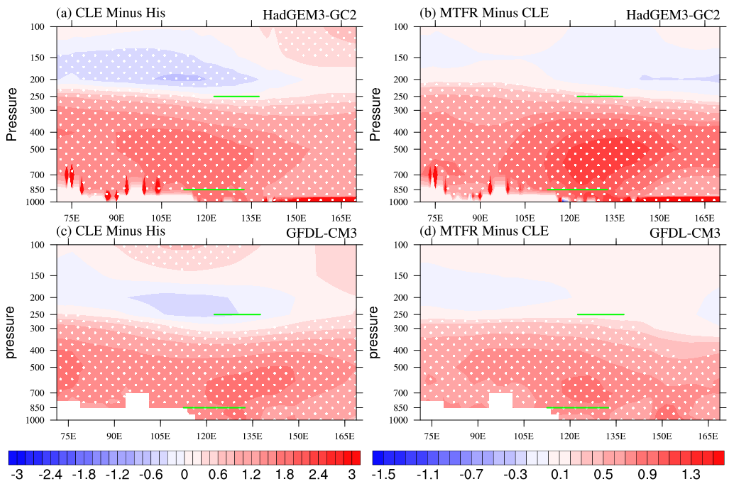

Fig.5 The difference in winter mean temperature (K) along 40°N (left) between CLE (2016-2049) and His (1980-2004), and (right) between MTFR (2016-2049) and CLE (2016-2049). The dotted areas are statistically significant at the 10% level. The green lines indicate the level and longitude used in the calculation of ΔT.

Deleted: 5

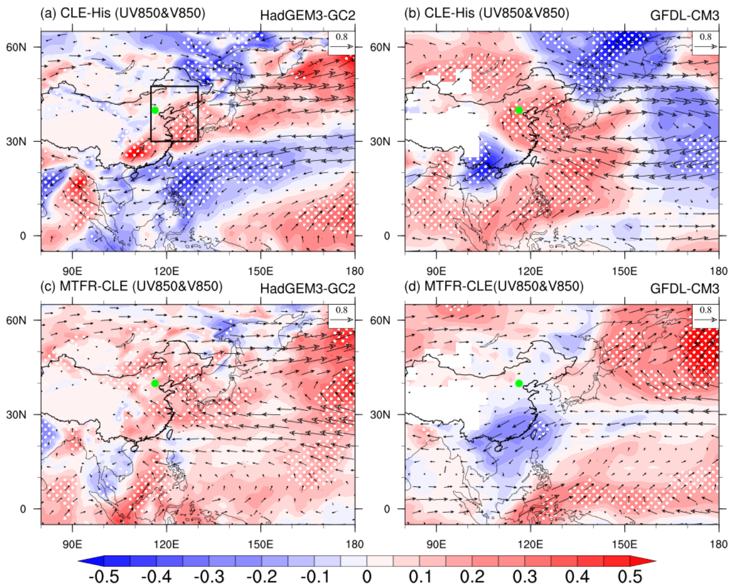

Fig. 6 Spatial distribution for the difference in winter mean 850 hPa winds (vector, m s^{-1}) and 850hPa meridional component (shading, m s^{-1}) (left) between CLE (2016-2049) and His (1980-2004), and (right) between MTFR (2016-2049) and CLE (2016-2049). The dotted areas denote the 850hPa meridional winds statistically significant at the 10% level. The black boxes indicate the region used in the calculation of V850.

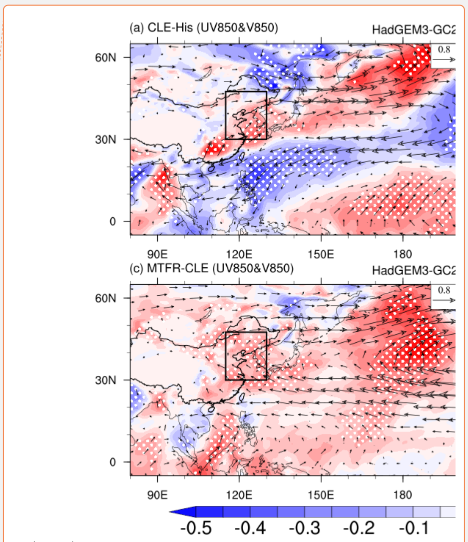

Deleted:

Formatted: Font:(Default) Times New Roman

Formatted: Centered

Deleted: **6**

Formatted: Font color: R,G,B (4,50,255)

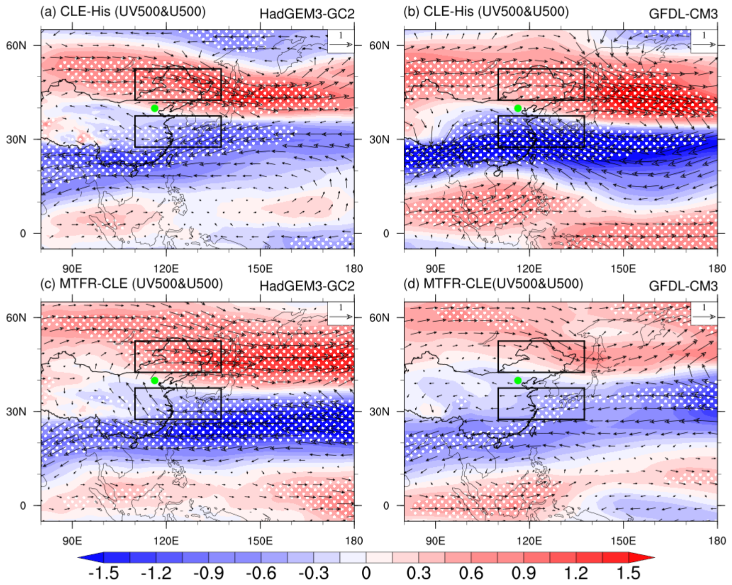

Fig. 7 Same as Fig. 6, but for the difference in 500hPa winds (vector, m s^{-1}) and 500hPa zonal component (shading, m s^{-1}). The black boxes indicate the regions used in the calculation of U500.

Deleted:

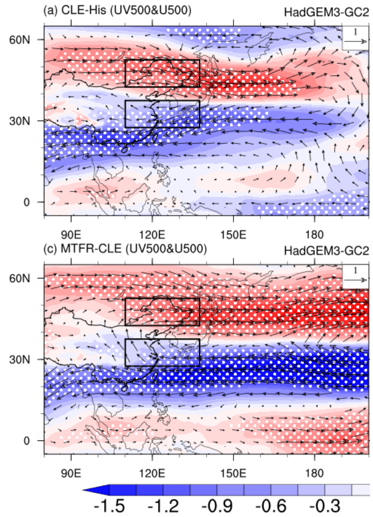

Formatted: Font: (Default) Times New Roman

Formatted: Centered

Deleted: 7

Deleted: 6

Formatted: Font color: R,G,B (4,50,255)

Deleted:

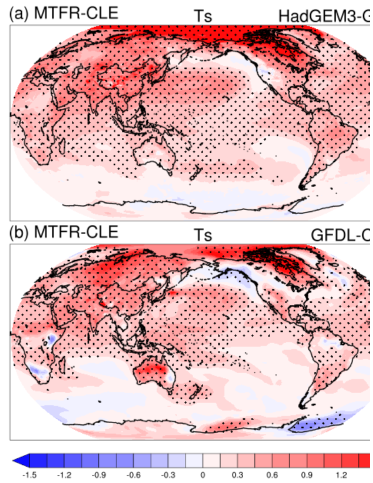

Formatted: Font: (Default) Times New Roman

Formatted: Centered

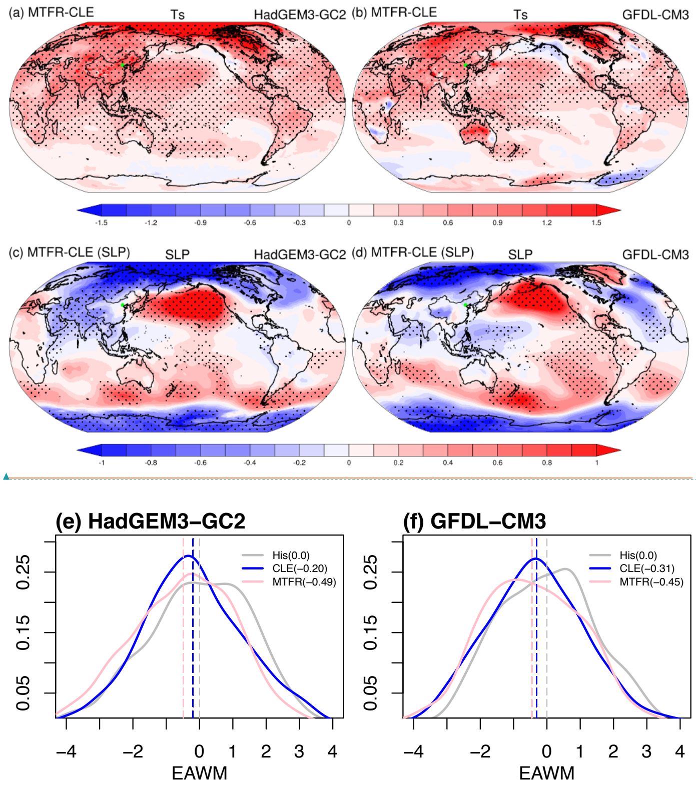

Fig.8 The difference of the climate mean surface temperature (left, K) and sea level pressure (right, hPa) between MTFR and CLE simulated by (a)-(b) HadGEM3-GC2 and (c)-(d) GFDL-CM3. The dotted areas in (a)-(d) are statistically significant at the 10% level using a Student's t-test. PDF via Kernel density estimation of EAWM in His (1980-2004, grey), CLE (2016-2050, blue) and MTFR (2016-2050, pink) simulated by (e) HadGEM3-GC2, and (f) GFDL-CM3. The numbers in (e)-(f) are the climate mean of EAWM.

Formatted: Font: (Default) Times New Roman

Formatted: Font: (Default) Times New Roman

Deleted:

Deleted: 8

Deleted:

Page Break

Formatted: Font: (Default) Times New Roman

Deleted: Page Break

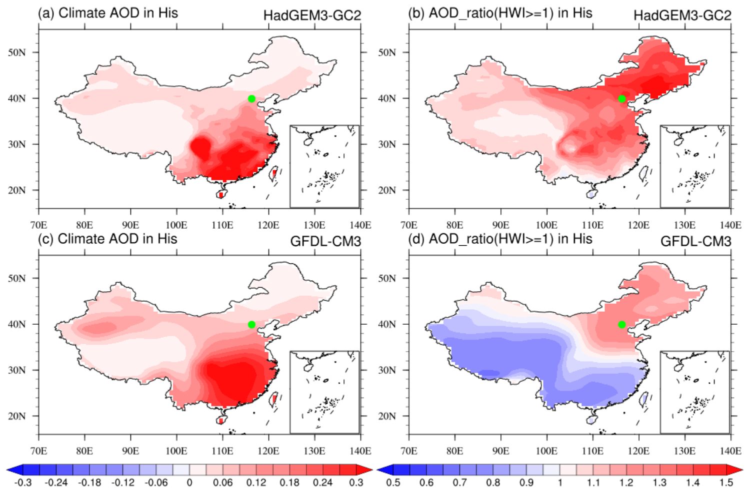

Fig. 9 Winter mean (left) AOD at 550 nm in (a) HadGEM3-GC2 and (c) GFDL-CM3 averaged over 1980-2004. Right is same as left, but for the mean AOD ratio of the winter months with HWI≥1 (hereafter AOD_ratio(HWI≥1) in His). Blue and red shadings in (b) and (d) are decreased and elevated AOD relative to the climate winter mean of His, respectively.

Deleted:

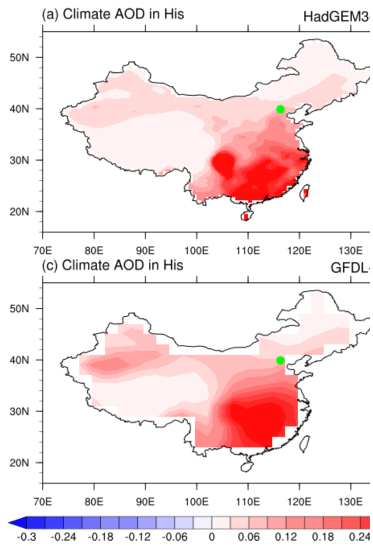

Formatted: Font:(Default) Times New Roman

Deleted: 10

Formatted: Font color: R,G,B (4,50,255)

Deleted: DJF

Deleted: n

Deleted: ratio of

Deleted: (unit: %) averaged

Deleted: in

Formatted: Font color: R,G,B (4,50,255)

Deleted:

Formatted: Font color: R,G,B (4,50,255)

Deleted: relative to winter mean of 1980-2004

Formatted: Font color: R,G,B (4,50,255)

Deleted: c

Deleted: -

Formatted: Font color: R,G,B (4,50,255)

Deleted: lower and higher than

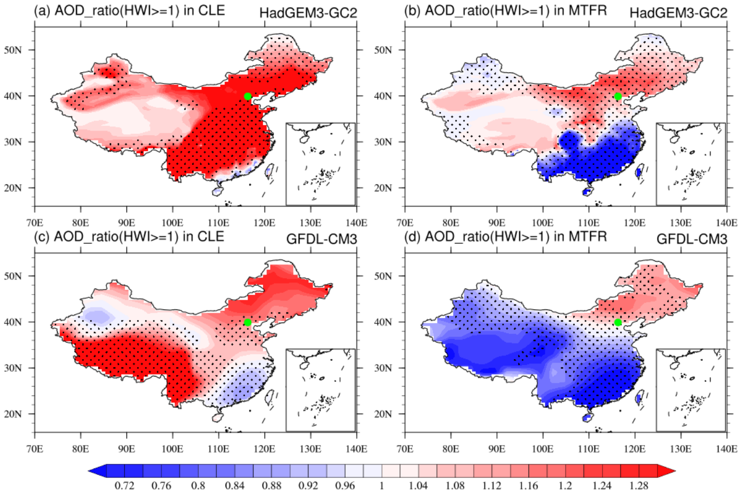

Fig 10. Same as Fig.9b and d, but for the results projected in CLE and MTFR. The dotted areas are statistically significant at the 10% level using a Student's t-test.

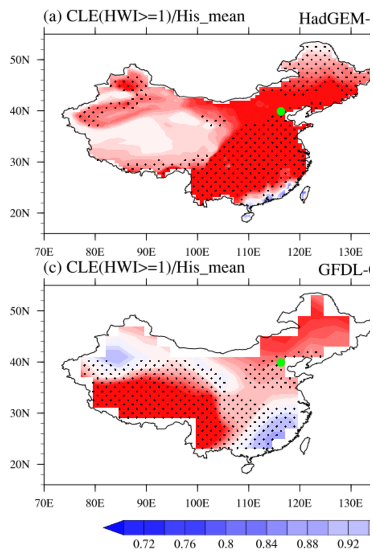

Deleted:

Formatted: Font:(Default) Times New Roman

Formatted: Centered

Deleted: **11**

Deleted: 10

Deleted: The baseline is the winter mean of 1980-2004.

Formatted: Left, Indent: Left: 0 cm, First line: 0 cm, Space Before: 0 pt, After: 0 pt, Line spacing: single

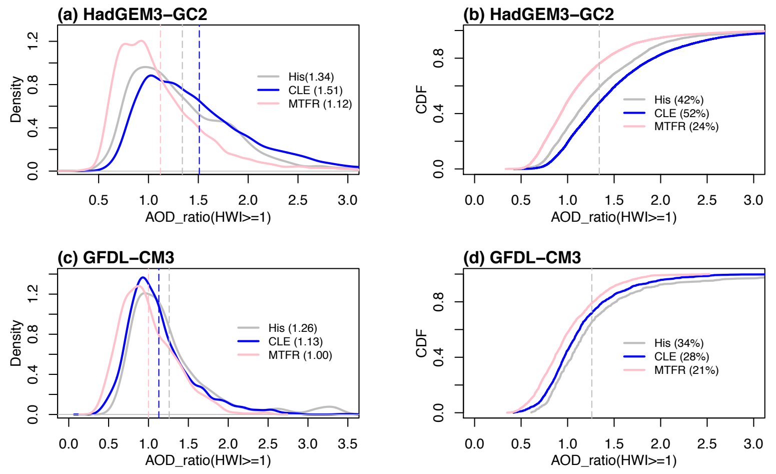

Fig.11 (a) PDF and (b) CDF distributions of AOD_ratio(HWI≥1) over North China (33-45°N, 105-122°E, box in Fig.2) in HadGEM3-GC2. (c)-(d) are the results from GFDL-CM3. The grey, blue and pink vertical lines and numbers in (a) and (c) are the winter mean AOD_ratio(HWI≥1) of His, CLE and MTFR, respectively. The numbers in (b) and (d) are the cumulative probability of AOD_ratio(HWI≥1) higher than the winter mean AOD_ratio(HWI≥1) of His.

Deleted: Fig.1

Formatted: Font:(Default) Times New Roman

Formatted: Font:(Default) Times New Roman

Formatted: Font:Bold, Font color: R,G,B (4,50,255)

Formatted: Font color: R,G,B (4,50,255)